Characterization of Electrochemically Deposited $Ce_{1-x}Zr_xO_2$ Layers Modified with Cobalt Oxide for Electrocatalytic Conversion of NO_x and CO

A. Tsanev,[a] P. Iliev,[b] K. Petrov,[b] P. Stefanov,[a] and D. Stoychev[c,*]

[a]Institute of General and Inorganic Chemistry – Bulgarian Academy of Sciences, 1113 Sofia, Acad. G. Bonchev Str., bl.11

[b]Institute of Electrochemistry and Energy Systems – Bulgarian Academy of Sciences, 1113 Sofia, Acad. G. Bonchev Str., bl.10

[c]Institute of Physical Chemistry Acad. R. Kaishev – Bulgarian Academy of Sciences, 1113 Sofia, Acad. G. Bonchev Str., bl.11

doi: 10.15255/CABEQ.2014.2017

Original scientific paper
Received: March 20, 2014
Accepted: September 5, 2014

A method for electrochemical deposition of a two-component $Ce_{1-x}Zr_xO_2$ system on stainless steel substrate that is attractive from catalytic point of view is proposed. As reported in the literature, it is a promising carrier layer for the production of catalytic converters for purification of exhaust gases containing NO_x and CO. This system is modified by electrodeposition of a thin film of cobalt oxide over it. A series of samples of the $Ce_{1-x}Zr_xO_2/Co_xO_y$ system was produced with various concentrations and proportions of the components. These samples are characterized by XRD, SEM, EDS, XPS and PCC (partial electrocatalytic curves) of CO oxidation and of NO_x reduction. Based on the obtained results, it has been concluded that the electrodeposited two-component $Ce_{1-x}Zr_xO_2$ system is a solid solution with composition, structure, and physicochemical properties that make it suitable for use as active phase carrier for catalytic oxidation of CO and reduction of NO_x.

Key words:
thin films, electrodeposition, $Ce_{1-x}Zr_xO_2$, electrocatalytic conversion, NO_x, CO

Introduction

In the last few decades, a significant increase in NO_x and CO emissions has been observed. These pollutant gas emissions are mostly the result of combustion processes in motor vehicles, as well as industrial and energy sector processes. In these processes, NO_x and CO may be released as a mixture or as separate gases.[1–5]

Several catalytic methods have been developed for NO_x reduction.[6] Direct decomposition is a simple and desirable way of removing NO_x, as no reducing agents or changes in driving cycles are required. This approach has been realized via electrochemical removal of NO_x.[7] The electrodes employed in the electrochemical reduction of NO and oxidation of CO are usually noble transition metals, since they are very active catalysts.[8–11]

In this communication, we present our results regarding the use of non-precious metal electrodes for both NO_x reduction and CO oxidation in a gas diffusion electrode (GDE). The investigated catalytic systems were obtained by electrochemical deposition of a $Ce_{1-x}Zr_xO_2$ layer on a stainless steel (SS 1.4301) mesh substrate, and then applying (again by electrochemical deposition) a second layer of cobalt oxide (Co_xO_y). Thus, the obtained catalytic systems were incorporated into hydrophobic GDEs.[12]

We have chosen this approach and the combination of electrochemically deposited carrier and active phase layers, because the mixed oxide $Ce_{1-x}Zr_xO_2$ is known to have high adsorption capacity with regard to NO_x due to the numerous centres of alkaline nature on its surface.[13] Furthermore, the additional cobalt oxide film over the $Ce_{1-x}Zr_xO_2$ layer is characterized by high activity in the catalytic reactions of NO_x-reduction[14] and CO-oxidation,[15–17] as well as removal of volatile organic compounds[18–20] because of the presence of mobile oxygen, i.e., unsupported cobalt oxide is an active catalyst in air pollution control for the abatement of CO and NO_x.[21]

The choice of GDE as the model microreactor for studying the catalytic activity of the systems of interest was based on some of its advantages as compared to standard catalytic reactors.[12] For instance, GDEs allow expansion of the catalyst-electrolyte-gas contact surface, which in turn guarantees optimum utilization of the working catalyst surface,[22] as well as elimination of any side-processes (including corrosion processes). This is because the catalytic layer is isolated from the electrolyte.[22]

*Corresponding author: e-mail: stoychev@ipchp.ipc.bas.bg; tel.: +359 2 979 25 29

In view of the above considerations, the aim of this study was to establish the feasibility of a fast and simple method that does not require expensive equipment to evaluate the reactions of NO_x reduction and CO oxidation, using GDE with incorporated electrochemically produced electrocatalytic active system $Co_xO_y/Ce_{1-x}Zr_xO_2/SS$.

Experimental

Substrates of dimensions 5 x 6 cm were cut from a 40 μm thick stainless steel mesh (SS 1.4301 – 18.2 % Cr, 8.1 % Ni, 1.5 % Mn, 0.37 % Si, 0.44 % C, 0.004 % S, 71.386 % Fe), which is a standard material commonly used in the assembly and manufacture of gas diffusion electrodes. The substrates were subjected to the following pre-treatment procedures: alkaline degreasing, and activation in acidic medium employing a standard procedure.[23] The electrochemical deposition of thin films (1–5 μm) of $Ce_{1-x}Zr_xO_2$ onto these substrates was conducted in electrolyte based on absolute ethyl alcohol with 10 g L^{-1} $ZrCl_4$ and various concentrations (from 80 to 140 g L^{-1}) of $CeCl_3$. A platinised titanium mesh was used as insoluble anode with an area of about 2.5 times that of the cathode. The oxide layers were electrodeposited in a potentiostatic regime at 8–10 V under continuous mechanical agitation of the solution. Because of the high specific electrical resistance of the electrolyte, the latter's temperature increased during the electrolytic process, which required its continuous cooling/thermostating to 8–10 °C, assumed to be the optimum temperature. The electrolytic process was conducted for 60–120 minutes, and then the samples were washed with distilled water, and dried in a flow of hot air. Specimens of appropriate size were cut from the prepared samples and subjected to XPS, SEM and EDS analyses.

On the remaining (larger) parts of the samples coated with $Ce_{1-x}Zr_xO_2$, a second layer (0.5–1.0 μm thick) of a mixture of Co_xO_y and $Co(OH)_2$ was deposited. The electrodeposition of this second layer was carried out in a galvanostatic regime (i = 4 mA cm^{-2}) in absolute ethyl alcohol based electrolyte containing 40 g L^{-1} $CoSO_4$. Again, specimens from thus prepared samples were cut and set to examination by XPS, SEM and EDS, and GDEs were fabricated from these samples (for the composition of the samples see Table 1).

The gas diffusion electrodes for the electrocatalytic studies were prepared employing the following procedure: A gas diffusion layer of hydrophobized acetylene black (hydrophobized with 45 % teflon) was pressed in the form of a tablet, at pressure p = 300 kg cm^{-2} and T = 300 °C, onto the steel mesh with the electrodeposited $Co_xO_y/Ce_{1-x}Zr_xO_2$ coating.

Table 1 – *Composition of the different $Ce_{1-x}Zr_xO_2$ layers and concentrations of additionally electrodeposited Co_xO_y on $Ce_{1-x}Zr_xO_2$ layers. In the separate columns are given oxidation/reduction potentials for CO and NO_x reactions, respectively, determined from partial polarization curves.*

№ of samples	Composition of layers' surface	Concentration of Co (at %)	Oxidation potential of CO (mV) at 1.5 mA cm^{-2}	Reduction potential of NO_x (mV) at 1.5 mA cm^{-2}
1	SS	0	467	–428
2.1	$Ce_{0.74}Zr_{0.26}O_2$	0	496	–184
2.2	$Ce_{0.74}Zr_{0.26}O_2$	91.5	520	–247
3	$Ce_{0.72}Zr_{0.28}O_2$	10.9	–	–
4	$Ce_{0.42}Zr_{0.58}O_2$	33.4	498	–270
5	$Ce_{0.27}Zr_{0.73}O_2$	0	398	–308
6	$Ce_{0.19}Zr_{0.81}O_2$	100	404	–188
7	$Ce_{0.11}Zr_{0.89}O_2$	97.9	288	–287
8	$Ce_{0.07}Zr_{0.93}O_2$	95.8	454	–603
9	$Ce_{0.02}Zr_{0.98}O_2$	97.7	467	–440
10	SS	100	464	–528

Under these particular assembly conditions, the entire amount of $Co(OH)_2$ is converted into Co_xO_y. Thus prepared GDEs were used to study the electrochemical characteristics of the $Co_xO_y/Ce_{1-x}Zr_xO_2/SS$ system with regard to the reactions of CO oxidation and NO_x reduction.

Used was a specially designed electrochemical cell (see Fig. 1[24]), which allowed gas supply from the acetylene black gas diffusion layer. The gases were supplied from bottles to the gas diffusion layer of the GDE.

A nickel "sponge" was used as counter electrode and the reference electrode was saturated calomel electrode (SCE). The process of CO oxidation was studied in 1 g L^{-1} K_2CO_3 aqueous solution, in

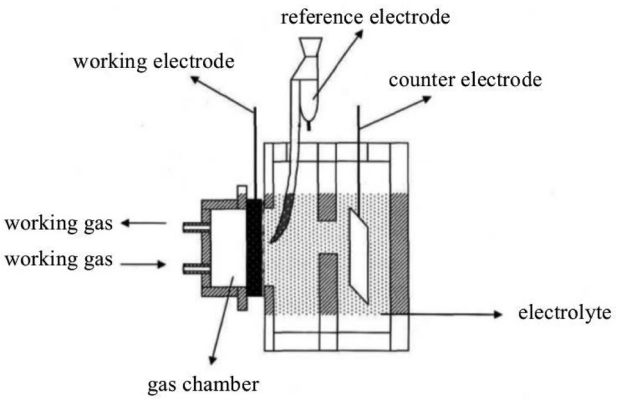

Fig. 1 – *Common scheme of the electrochemical cell/GDE used in the electrocatalytical experiments*

which CO entered and passed through the diffusion layer of the GDE, provided from a gas bottle. The process of the NO_x reduction was studied in 1 g L^{-1} KNO_3 aqueous solution in which NO_x entered and again passed through the diffusion layer of the GDE provided from a gas bottle. A potentiostat/galvanostat Solartron 1286 was used to plot the stationary volt-ampere curves for the studied processes.

The structure and phase composition of electrochemically deposited films were identified by X-ray diffraction (XRD) analysis with a Philips diffractometer (equipped with a secondary monochromator) using Cu K_α radiation. The acquisition conditions were 2θ from 20 to 80°.

The surface morphology of the samples was examined by scanning electron microscopy using a JEOL JSM 6390 electron microscope (Japan) equipped with an ultrahigh resolution scanning system in a regime of secondary electron image (SEI) and an INCA energy-dispersive X-ray spectrometer (EDS). The accelerating voltage was 25 kV, I~ 65 mA. The vacuum was 10^{-6} Torr.

The chemical states and elemental composition of the layers were investigated by XPS. These were carried out by means of a VG Escalab Mk II spectrometer (England) using an Al K_α excitation source (1486.6 eV) with a total instrumental resolution of ~1 eV, under a base pressure of $1 \cdot 10^{-8}$ Pa. The O 1s, Ce 3d, Zr 3d, Y 3d and Co2p photoelectron lines were calibrated to the C 1s line. The surface composition of the mixed oxide layers was determined from the ratio of the corresponding peak areas, corrected with the photoionization cross sections.[25]

Results

XRD analyses

XRD-analyses were performed on $Ce_{1-x}Zr_xO_2$ layers electrodeposited on dense stainless steel (SS 1.4301) substrate (specimen), obtained at conditions, similar to those used for the deposition of the same $Ce_{1-x}Zr_xO_2$ layers on steel mesh. This approach was prompted by the fact that highly uneven surface of the real samples obtained on stainless steel mesh did not allow the acquisition of correct X-ray diffraction results. Again, as deposited and pre-heated (to 300 °C, for 2 hours) specimen $Ce_{1-x}Zr_xO_2$/SS were examined (under conditions analogous to the conditions of GDE pressing).

Fig. 2 (No. I) shows that the reflexes of the as-deposited samples in the XRD pattern are characterized by large half-width of all reflexes, which is an indication of the presence of phases built of small-sized particles ensuring larger "working" surface of the deposited phase. In an attempt to obtain more accurate peak indexing for the detected

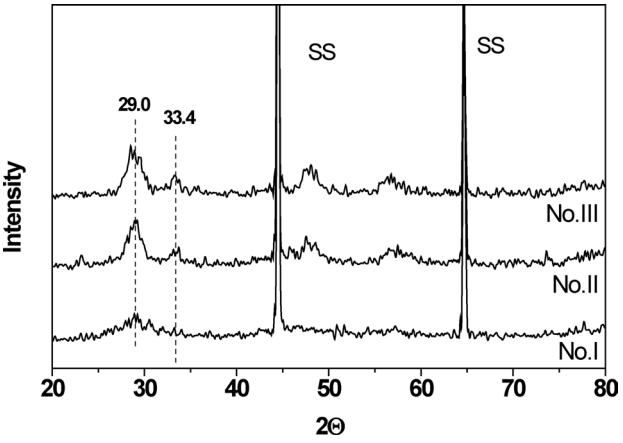

Fig. 2 – *XRD-analysis of the $Ce_{1-x}Zr_xO_2$ layers, electrodeposited on stainless steel for sample No. I (as-deposited), where Zr/Ce = 4; for sample No. II (after annealing), where Zr/Ce = 0.77; for sample No. III (after annealing), where Zr/Ce = 0.76*

phases, we performed XRD analysis of the same samples after annealing at 500 °C for 2 hours (Fig. 2, No.II and No.III). All the profiles (except those for Fe from the substrate) are typical of cubic cerium dioxide.[26] The reflexes at 28.6° and at 33.1°, characteristic of cubic cerium dioxide,[26] are shifted towards larger angles (29.0° and 33.4°, respectively), which may be attributed to incorporation of zirconium dioxide into cerium dioxide crystal lattice and formation of a solid.[26] These results indicate that the electrochemical method of deposition of the system $Ce_{1-x}Zr_xO_2$, like other methods, too, produces a solid solution.

SEM and EDS studies

The surface morphology of the electrochemically deposited $Ce_{1-x}Zr_xO_2$ layers were set to SEM examinations before the deposition of cobalt oxide film on their surface (Fig. 3). The SEM image shows that the $Ce_{1-x}Zr_xO_2$ layers are cracked but have good adhesion to the substrate (Fig. 3a – sample No. 2.1 (for the composition of the samples see Table 1). Two types of zones are visible, smooth and cracked. EDS analyses (regarding the amount of registered Fe – from SS substrate – that is an indication for thickness of the overlayer) shows that the layer in the smooth zones is thinner, more compact and uninterrupted, whereas in the cracked zones, it is thicker (reaching a thickness of about 3–5 μm). A characteristic picture of the thicker zones is presented in Fig. 3b (sample No. 2.1), and of the smoother zones, in Fig. 3c (sample No. 2.1).

The substantial difference between the two types of zones is determined by the non-homogeneous surface of the substrate, including roughness (at the binding sites between the mesh fibres) and other defects. It can be clearly seen in Fig. 3a that

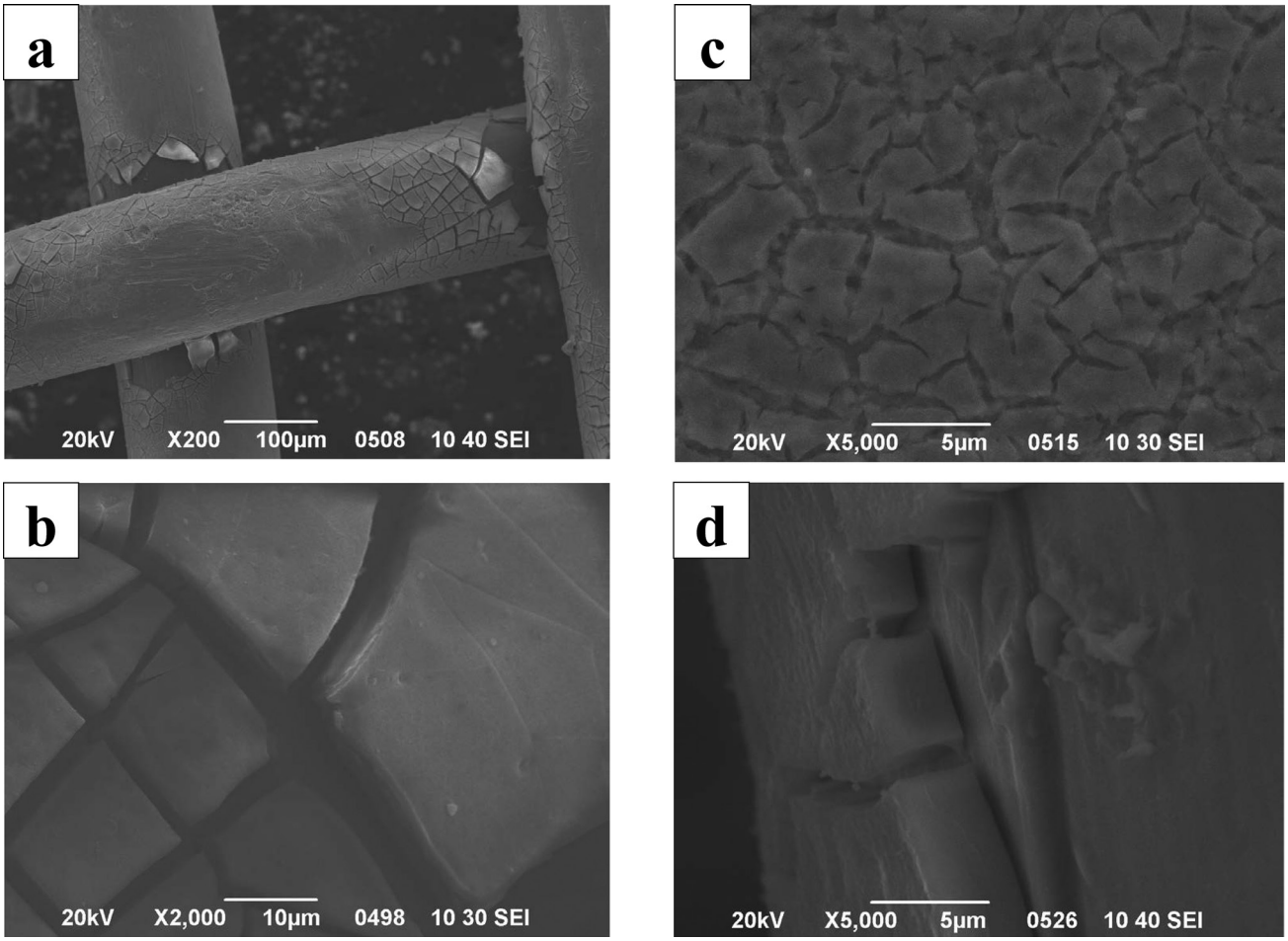

Fig. 3 – *SEM micrographs of the $Ce_{1-x}Zr_xO_2$ layers (for sample No.2.1) before electrodeposition of cobalt oxide layers at different magnifications – a – 200x; b – 2000x; c – 5000x; d – 5000x*

the layer formed at the sites where two fibres overlap is considerably thinner, which may be related to a more intense evolution of hydrogen in these zones and hence impeded growth of a denser layer. The thickness of the deposited layer in these zones was estimated to be about 2.5 – 5 µm (Fig. 3d, sample No. 2.1).

A quantitative evaluation of the elemental composition of the $Ce_{1-x}Zr_xO_2$ carrier layer was performed by energy-dispersive spectroscopy (EDS). The integral EDS analysis of the surface corresponding to the area photographed at 1000x magnification (Fig. 4, sample No. 2.1) indicates predominantly the presence of cerium oxide. The peaks for zirconium oxide in the EDS spectra are of low intensity, which makes accurate determination, respective calculation of their real quantity in the system difficult by this method. Certain amounts of chlorine were also detected which may be related to included chlorine ions, a component of the electroplating bath solution. According to the obtained EDS data, the elemental composition of the carrier layer is 2.9 at. % Zr, 13.3 at. % Ce, and 83.8 at. % O.

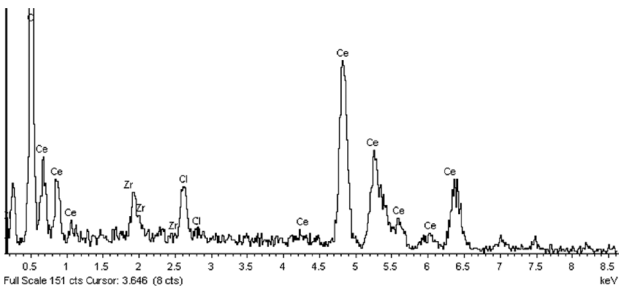

Fig. 4 – *EDS-analysis of $Ce_{1-x}Zr_xO_2$ layer (for sample No. 2.1)*

The EDS analyses at higher magnifications (2000x) recording information from zones with thicker layers (the signal in these zones being obtained from larger area/volume), give considerably higher content of zirconium in the system, the Zr/Ce ratio reaching a value of 0.6. Analogous analysis at higher microscope image magnifications have established unambiguously the presence of a layer composed mostly of cerium oxide at the bottom of the cracks, which is evidence that the $Ce_{1-x}Zr_xO_2$ layer formed on the steel mesh is uninterrupted.

The cobalt oxide coated $Ce_{1-x}Zr_xO_2$ layers were also subjected to SEM analysis. The obtained SEM images indicate clearly that it is possible to change

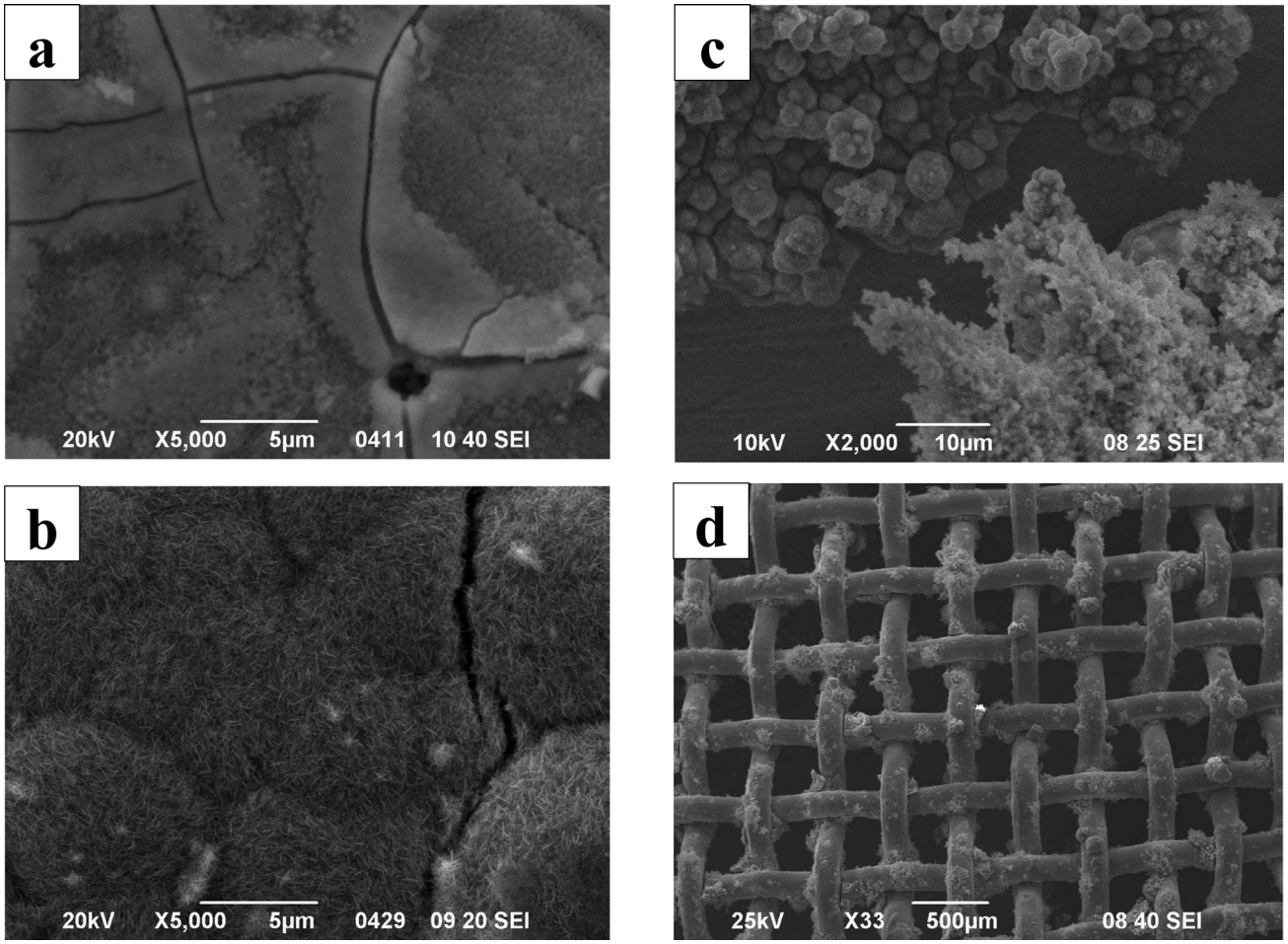

Fig. 5 – *SEM micrographs of the cobalt oxide layers for samples: a – No.8 (5000x); b – No.7 – (5000x); c – No.2.2 (2000x), d – No.2.2 (33x)*

the morphology of the electrodeposited cobalt oxide layer by varying the conditions of electrodeposition (in our case increasing cathode current density and/or increasing electrolyte`s temperature). A typical picture of the formed cobalt oxide layer is presented in Fig. 5a (sample No. 8). The SEM image shows that the homogeneous surface of the cobalt oxide coating, too, is cracked in certain zones. When observed in the backscattered electron imaging (BEI) mode, the peripheral zones of the cracks feature lighter areas. EDS analysis of these zones indicates that they are richer in cerium oxide and the cobalt layer is deposited predominantly between these zones.

A very different picture is obtained for sample No. 7 (which, as will be reported further in this paper, has proved to be most active in the reaction of CO oxidation – Fig. 5b). The morphology of this sample is characterized by a needle-like structure of the cobalt oxide layer providing high specific surface of the layer.

A highly developed surface of the cobalt oxide layer has also been registered for sample No. 2.2 (Fig. 5 c, d). In this case, two types of structural forms such as spheroid agglomerates and dendrite zones are formed on the agglomerates. These results suggest the presence of two different cobalt phases.

XPS studies

The qualitative and quantitative composition of the electrodeposited layers was studied by XPS (Table 1). Fig. 6 a, b presents the recorded Zr3d and Ce3d spectra for the studied samples before electrodeposition of the cobalt oxide layer. The spectra are of weak intensity, due to the fact that the layers are deposited on a mesh, i.e. the scanning surface is relatively small.

The Zr3d spectra (Fig. 6a) are typical of Zr^{4+} oxidation state.[27] The positions of $Zr3d_{3/2}$ and $Zr3d_{5/2}$ peaks are at 182.8 eV and 185.2 eV, respectively, with a spin-orbit splitting of 2.4 eV between them. The constant value of the binding energy between $Zr3d_{3/2}$ and $Zr3d_{5/2}$ indicates a constant zirconium oxidation state independent of composition.

Fig. 6b shows the spectra of Ce3d. Only the spectrum for sample No 2.1 is more intense. The

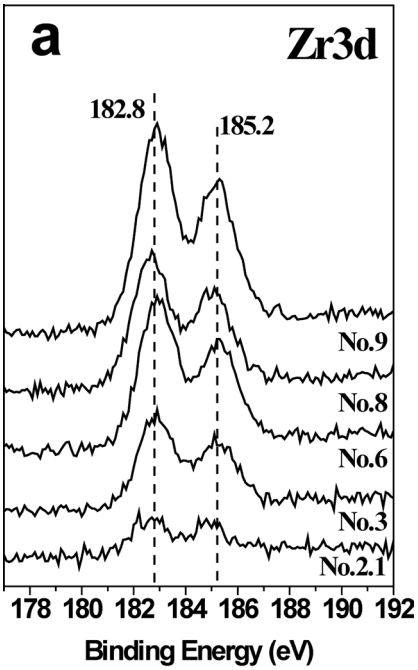

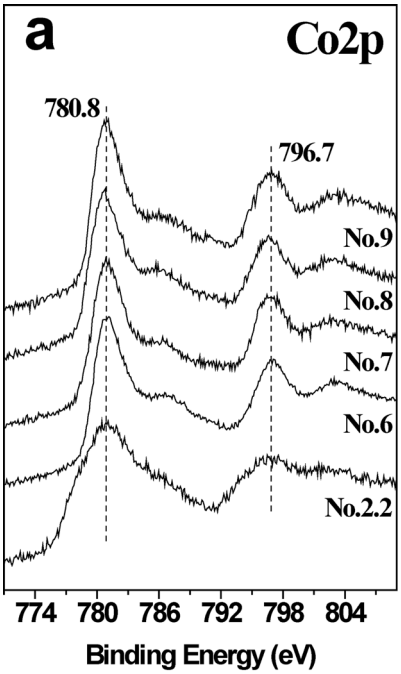

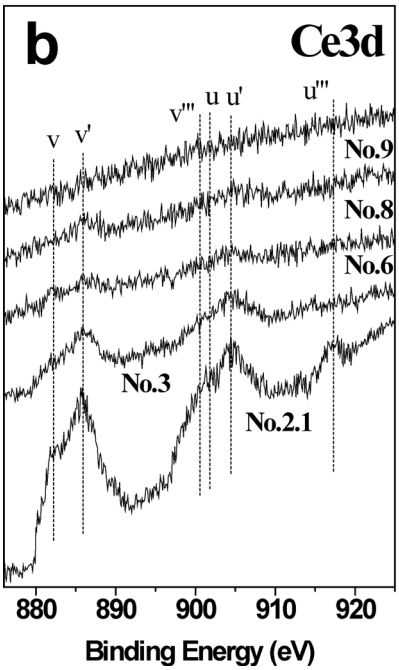

Fig. 6 – *XPS spectra of Zr3d (a) and Ce3d (b) for the different samples (see Table 1)*

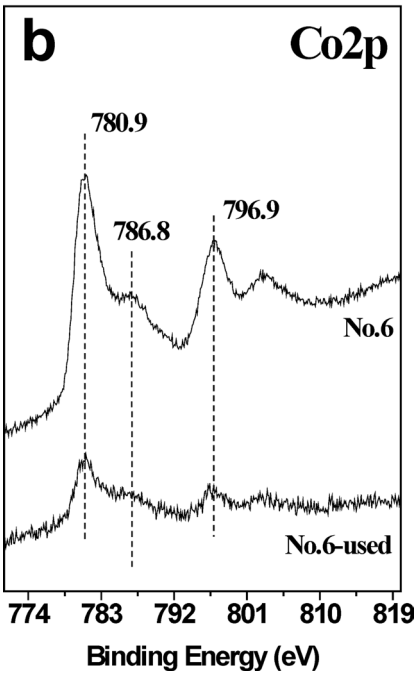

Fig. 7 – *XPS spectra of Co2p for as-deposited (a) and used (b) electrodes*

Ce3d spectra of all $Ce_{1-x}Zr_xO_2$ layers for all studied samples indicate the presence of cerium oxide. Moreover, the characteristic peak at 916.7 eV suggests the presence of a mixture of Ce^{3+} and Ce^{4+} oxidation states.

Fig. 7a presents the Co2p spectra for the studied as-deposited samples. The observed intense satellite peak, binding energy of the $Co2p_{3/2}$ peak at 780.9 eV, $Co2p_{3/2}$-$Co2p_{1/2}$ distance of 15.9 eV, and satellite-primary peak distance of 6.1 eV, indicate that the chemical state of cobalt is the same in all studied samples, the layers being a mixture of Co_2O_3 and $Co(OH)_2$.[28]

The XPS spectra of used electrodes were also recorded with the aim to follow the changes in the oxidation state of the catalytic layer (Fig. 7b). For this purpose, the tablet of hydrophobized acetylene black with the pressed on mesh with catalytic layer was mechanically removed and the used layer was analyzed.

A comparison between the two Co2p spectra, for as-deposited and used electrodes (Fig. 7b) shows

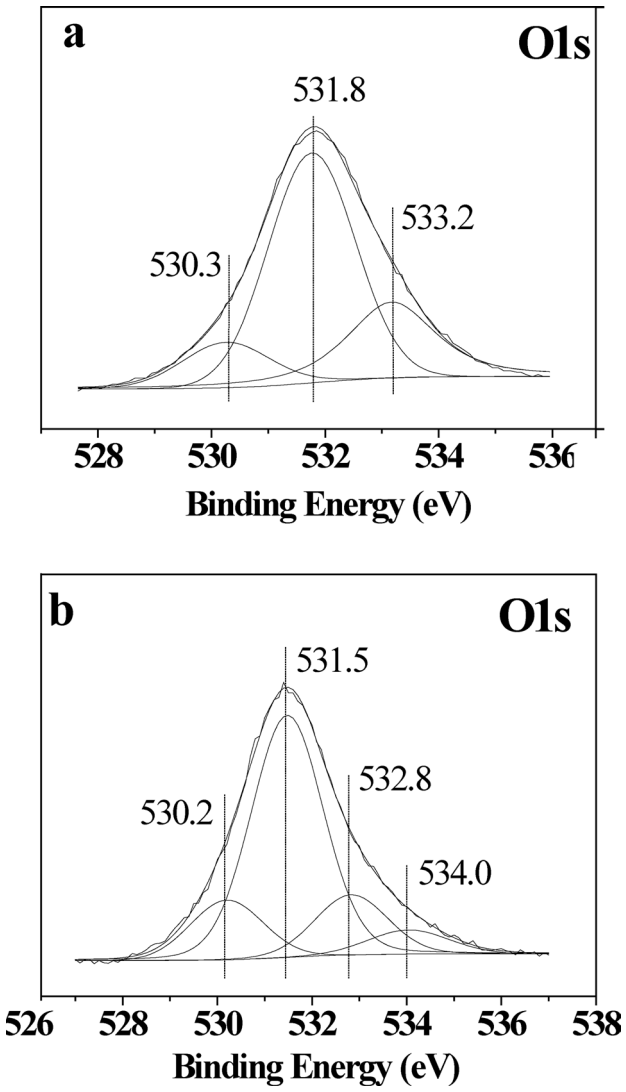

Fig. 8 – *Curve fitting of XPS spectra of O1s in the cobalt oxide layer for as-deposited (a) and used (b) electrodes*

that the oxidation state of the cobalt layer had not changed substantially after the use of the electrode. The Co2p spectrum for the used electrode is less intense because of the presence of residual acetylene black on its surface, which screens the photoelectron signal.

The oxygen O1s spectra for as-deposited samples (of the fresh produced layer) and for used sample, modified with cobalt oxide layer, practically do not differ in shape. Curve fitting of the XPS spectra (Fig. 8 a, b) yields three peaks: at 530.3 eV, 531.8 eV and 533.2 eV, corresponding to the oxygen atoms in Co_2O_3, $Co(OH)_2$ and adsorbed water, respectively.[29]

The curve fitted spectrum of O1s for used sample (Fig. 8b) features four peaks at 530.2 eV, 531.5 eV, 532.8 eV, and 534.0 eV.

The peak at 529.9 eV reflects the presence of oxygen atoms in Co_2O_3.[30] A quantitative indication for the content of the two elements is that the ratio between the peak areas for cobalt and oxygen is approximately 1:1.7. The most intense peak at 531.3 eV corresponds to carbon-bonded oxygen in the form of carbonates,[31] adsorbed on the teflon layer during operation of the electrode in K_2CO_3 containing electrolyte. The peak at 532.6 eV is related to nitrogen oxides adsorbed on the teflon layer in the course of the experiment, as well as to bonded nitrogen in traces of KNO_3.[32] The peak at 533.9 eV corresponds to oxygen in water.[33]

The obtained XPS data and the juxtaposition of the oxygen spectra for as-deposited and used samples give us grounds to conclude that no substantial changes have occurred in the catalytic layers of cobalt oxides as a result of their operation.

Electrocatalytic studies

Oxidation of CO and reduction of NO_x are processes that have been extensively studied in heterogeneous catalysis.[8,11] In view of the standard electrochemical potentials of the two reactions and taking into account the difference between them, we assumed that there was a thermodynamic probability for the two reactions to proceed via a purely electrochemical mechanism as well. On the other hand, it is well known that, at the same potential, the rate of the electrochemical reactions depends on several factors, including the nature of the electrode materials. In this connection, we set ourselves the task to study these reactions from an electrochemical point of view and investigate the effect of the chemical composition of the electrodeposited oxide layers.

Fig. 9a compares few representative voltage – current (V-A) curves of the studied electrodes with regard to the reaction of CO oxidation. The reaction proceeds at the lowest oxidation potentials on electrodes No. 7 and 6, and at the highest potentials, on electrodes No. 2.1 and 2.2 (i.e. $Ce_{0.74}Zr_{0.26}O_2$ layer modified or non-modified with cobalt oxide, Table 1). An analogous behaviour of similar systems has been observed earlier for the reaction of oxygen evolution.[34]

The same analytical procedure was also employed to evaluate the electrocatalytic activity of the studied electrodes for the reaction of NO_x reduction. The obtained results are presented in Fig. 9b. The lowest reduction potential values (at i = 1.5 mA cm^{-2}) are measured for sample electrodes No. 2.1 (non-modified with cobalt oxide) and No 6 with fully overlapping polarization curves. Electrode No. 8 is characterized by the highest reduction potential, and that of electrode No. 7 is in between, but the latter electrode is most efficient for the reaction of CO oxidation. The data in Fig. 9 indicate that, in contrast to the case of CO oxidation, modification of the $Ce_{1-x}Zr_xO_2$ layer with cobalt oxide even wors-

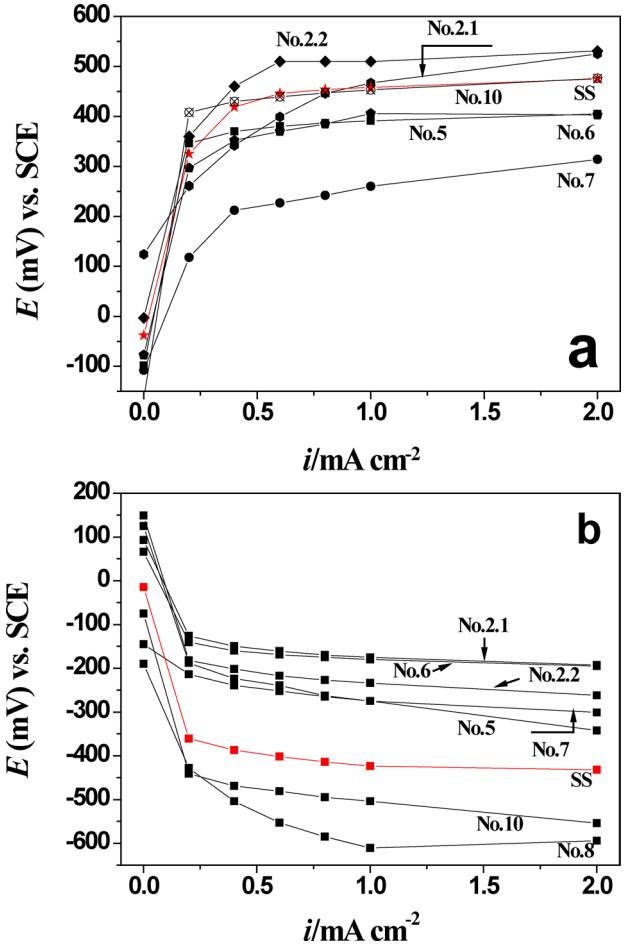

Fig. 9 – *Partial polarization curves showing comparison of the electrocatalytical curves of CO oxidation (a) and NO_x reduction (b) for the different electrodes (numbering is according Table 1)*

ens the catalytic activity of this electrode for NO_x reduction (curve 2.1).

In view of the previously discussed results, it was important to determine the impact of the ratio between the components of the $Ce_{1-x}Zr_xO_2$ system on these reactions. For this purpose, $Ce_{1-x}Zr_xO_2$ layers with various (high or low) content of cerium oxide were electrodeposited on SS without being modified with cobalt oxide. The results are summarised in Table 1. A comparison between the obtained partial polarization electrocatalytic curves for samples No. 2.1 (with high cerium oxide content) and No. 5 (with low cerium oxide content) for the reaction of NO_x reduction (Fig. 9b) gives us grounds to conclude that an increase in the content of cerium oxide in the layers leads to improvement of the electrocatalytic properties of the system with regard to NO_x reduction. Obviously, this effect of cerium oxide is related to lowering the potential at which the latter reaction proceeds. An indication in support of this conjecture is the potential difference between sample electrode No. 2.1 and stainless steel amounting to 244 mV (Fig 9b). In contrast, the obtained experimental data for the reaction of CO oxidation (Fig. 9a) show that increased concentration of cerium oxide in the layer has a negative effect on this reaction. The highest catalytic effect for the reaction of CO oxidation is observed with sample electrode No. 7 characterized by lower cerium oxide content in the $Ce_{1-x}Zr_xO_2$ system, which is further modified by an electrodeposited cobalt oxide layer on its surface. SEM data for this sample suggests a very well developed surface of the cobalt oxide layer, an effect that facilitates the formation of a greater number of active centres. Obviously, the well-developed specific surface of the $SS/Ce_{1-x}Zr_xO_2/Co_xO_y$ electrode will compensate for the impeded transport (supply, respectively) of oxygen ions and will thus facilitate reaction (electrode No. 8). The difference in CO conversion potential for sample electrode No. 7 and that for the uncoated stainless steel substrate is 179 mV, which indicates a substantial decrease in the energy threshold barrier for this reaction in the presence of the catalytic oxide $Ce_{1-x}Zr_xO_2/CoO$ system.

The possible reactions that may take place when modelling an electrocatalytic process of NO_x reduction and CO oxidation in the selected electrolytes are as follows:[35]

(I) NO_x reduction in aqueous solution of KNO_3:

$$2NO_2 + 8H^+ + 8e^- \rightleftharpoons N_2 + 4H_2O \quad (1)$$

$$2NO + 4H^+ + 4e^- \rightleftharpoons N_2 + 2H_2O \quad (2)$$

$$N_2O + 2H^+ + 2e^- \rightleftharpoons N_2 + H_2O \quad (3)$$

(II) CO oxidation in aqueous solution of K_2CO_3:

$$HCO_2H + H_2O \rightleftharpoons H_2CO_3 + 2H^+ + 2e^- \quad (4)$$

The above assumption that the reactions of NO_x reduction will proceed via the above described mechanism is also supported by the Pourbaix diagrams.[36]

Conclusions about possible reactions can be made based on Tafel slopes. Figure 10a presents the Tafel plots for the reactions of CO oxidation at current densities within the range 1–10 mA cm^{-2}. We have determined the values of the constant *b* for the Tafel equation (for each of the studied electrodes) from the slopes of the respective curves. It can be seen that the slopes of the Tafel curves for sample electrodes No. 6, 9 and 2.1 are close in value ($b \sim 130$ mV dec^{-1}), which corresponds to two-electron transfer reaction of oxidation of $C^{2+}O$ to $C^{4+}O_2$ (reaction 4).

Fig. 10b shows the Tafel plots for the reactions of NO_x reduction at current densities within the range 1–10 mA cm^{-2}. The Tafel curve for sample No. 6 is not presented in the figure because it over-

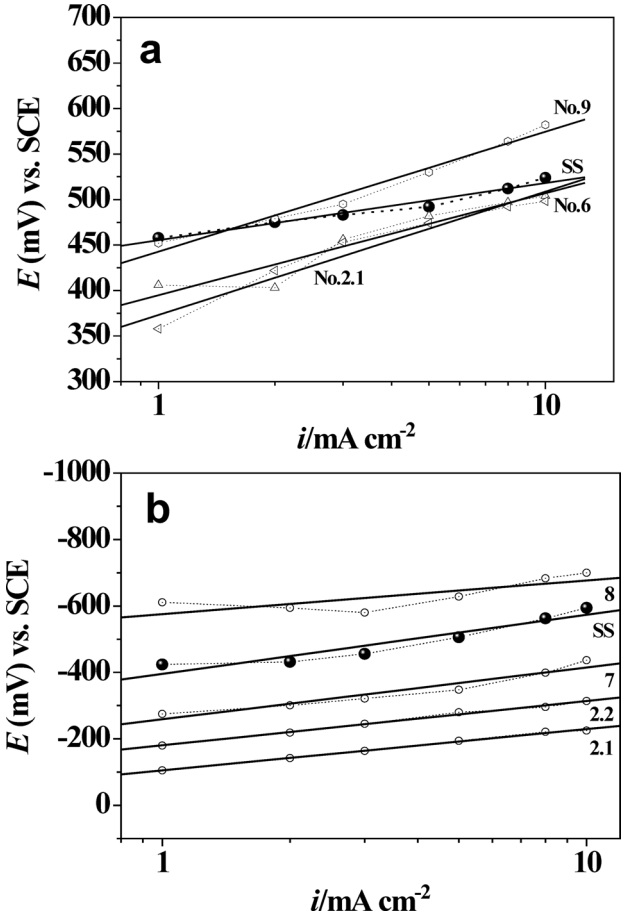

Fig. 10 – *Tafel curves for reactions of CO oxidation (at i = 1–10 mA cm^{-2}) and NO_x reduction (at i = 1–10 mA cm^{-2}) for the different electrodes*

laps fully with that of sample 2.1, i.e. the two-component oxide system with no cobalt layer deposited on it. In this case, the *b* constants for the Tafel equation for different electrodes, except for the steel electrode, are very close and equal to about 100–124 mV, which again leads us to two-electron transfers (reactions 1 – 3).

Simultaneous CO oxidation and NO_x reduction

On the base of the above results and following the additivity principle,[37] we studied the partial electrocatalytic curves (potentiostatic polarization curves – PPC) of CO oxidation and NO_x reduction. The obtained results are presented in Fig. 11 (curves for sample No. 2.2 – Fig. 11 a, b, respectively). The cross point between the partial curves (Fig. 11 – the point – "►") gives the mixed current ("short-circuit current") and mixed potential values for the two reactions. As evident from the figure, the established current values are very low (about 0.1 mA cm^{-2}), which allows analysis of the electrocatalytic curves at low current densities (i < 2 mA cm^{-2}). The similarity between measured and calculated mixed potentials is an indication for electrochemical mecha-

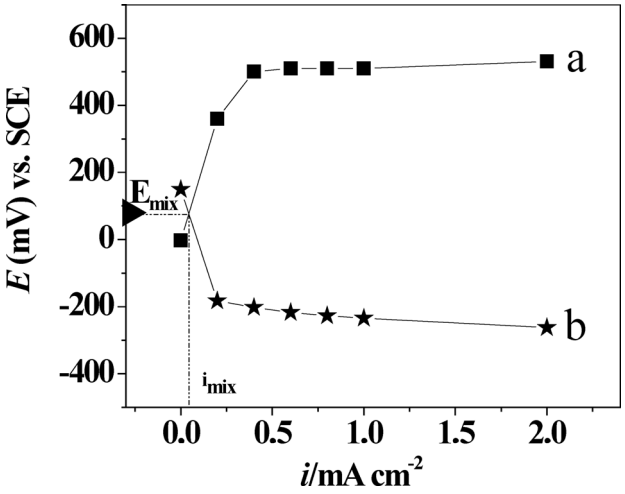

Fig. 11 – *Partial polarization curves of CO reduction (a) and NO_x oxidation (b) for sample number 2.2. The represented two curves are taken separately by two independent experiments.*

nism of the reaction. To prove the mechanism, quantitative measurement is necessary of the rate of the overall reaction. Unfortunately, this was not possible within the present study because of the small amounts of gas released in this particular experimental cell design.

Discussion

De Vooys *et al.*[8,38] report that in H_2SO_4 electrolytes purged with NO, the following products are obtained as a result of NO_x reduction:

1. In the potential region 0–0.3 V vs SHE, the main product of NO reduction is NH_3;
2. In the potential region 0.3–0.7 V vs SHE, the reaction product is N_2O;
3. Some nitrogen (N_2) is formed in the intermediate potential region (0.2–0.4 V vs SHE).

It should be born in mind however that the reaction of NO_x reduction is apparently quite sensitive to the nature of the electrode surface. Studies performed by Haneda and collaborators[14] show that the use of $Ce_{1-x}Zr_xO_2$ obtained from sol-gel as catalytically active systems may change radically the mechanism of the reaction of NO_x reduction. Because of its adsorption on the surface, NO is oxidized to NO_2 with formation of intermediate particles of nitrate (NO_3^-) species that are adsorbed on the surface of the Ce^{4+}–O^{2-} pair sites.

The established two-electron transfer involved in the reactions of NO_x reduction for the systems studied by us gives us grounds to presume that the mechanism of these reactions is close to the one proposed by Haneda *et al.*, i.e. NO_x reduction proceeds with evolution of nitrogen.

It is also obvious that modification with cobalt oxide has no catalytic effect as claimed in.[39–41] The oxidation potentials for samples No. 2.1 and No. 2.2 ($Ce_{0.74}Zr_{0.26}O_2$ layers modified or non-modified with cobalt oxide) did not differ much in value: 496 mV for sample No. 2.1, and 520 mV for sample No. 2.2, respectively. The established differences characterize the non-modified sample as more catalytically active.

In an attempt to verify the lack of "own" catalytic effect of the cobalt oxide layer, the electrocatalytic curves for CO oxidation and NO_x reduction were plotted also for a cobalt layer deposited on a steel substrate (sample No. 10). The obtained results show unambiguously that the electrodeposited cobalt oxide layer have no catalytic effect on these reactions. The electrocatalytic curve for the reaction of CO oxidation for sample No. 10 coincides fully with that for Co oxidation on steel. The experimental data for the reduction of NO_x suggest again (as for samples No. 2.1 and No. 2.2) that the cobalt oxide layer even has an inhibiting effect on this reaction.

In this respect, the only exception among the studied systems is electrode No. 7. This electrode exhibits the highest activity towards the reaction of CO oxidation as well as the best catalytic properties with regard to the reaction of NO_x reduction.

XPS and SEM analyses of modifying cobalt oxide layers indicate formation of a mixture of Co_2O_3 and $Co(OH)_2$ in these layers during their formation. In our opinion, it is highly probable that (under these particular conditions of GDE tablet assembly, i.e. high temperature (300 °C) and oxygen deficiency) the $Co(OH)_2$ in the layer will be converted into CoO according to the following reaction:[42]

$$Co(OH)_2 \xrightarrow{\Delta} CoO + H_2O. \qquad (5)$$

On sample stay in the air and/or when immersed in the electrolyte, however, the superficial CoO layer might be transformed back to $Co(OH)_2$[42] and thus exert a negative effect on the catalytic activity of the layer.

Conclusions

Various combinations of the $Ce_{1-x}Zr_xO_2$ system are electrochemically obtained and systematically characterized by XPS, XRD, SEM and EDS analyses. Based on the obtained results, it is concluded that the electrodeposited two-component $Ce_{1-x}Zr_xO_2$ system is a solid solution with composition, structure and physical-chemical properties that make it suitable for use as active phase carrier for catalytic CO oxidation of and NO_x reduction.

The catalytic activity towards the above reactions of thus produced $Ce_{1-x}Zr_xO_2$ layers, modified with cobalt oxide, is studied by incorporating them as the basic component in hydrophobous gas diffusion electrodes. The following conclusions are drawn on the grounds of the obtained experimental results:

The rate determining stage in the studied processes is the transport of oxygen;

Both reactions, CO oxidation and NO_x reduction, involve two-electron transfers, which is in agreement with the oxidation and reduction mechanisms proposed by other authors;

Based on the results from electrocatalytic characterization of the electrodeposited $Ce_{1-x}Zr_xO_2$ system, it is confirmed that it plays a significant catalytic role in the reactions involving oxygen;

The obtained XPS data suggest no substantial changes in the oxidation state of the $Ce_{1-x}Zr_xO_2/Co_xO_y$ system as a result of the oxidation-reduction reactions, which indicates that no side reactions proceed with involvement of this system;

Electrochemically obtained $Ce_{1-x}Zr_xO_2/Co_xO_y$ system is applicable and promising for direct reduction of NO_x and, in certain cases, for oxidation of CO.

References

1. *Tran, K.-Q., Kilpinen, P., Kumar, N.,* Appl. Catal. B Env. **78** (2008) 129. http://dx.doi.org/10.1016/j.apcatb.2007.09.004
2. *Kunming, J. I. A., Huili, Z., Wencui, L.,* Chi. J. Catal. **29** (11) (2008) 1089. http://dx.doi.org/10.1016/S1872–2067(09)60006–1
3. *Bera, P., Hegde, M. S.,* J. Indian Inst. Sci. **90** (2010) 299.
4. *Bera, P., Hegde, M. S.,* Catal. Surveys Asia **15** (2011) 181.
5. *Taylor, K.,* Catal. Rev. Sci. Eng. **35** (1993) 457. http://dx.doi.org/10.1080/01614949308013915
6. *Roy, S., Hegde, M. S., Madras, G.,* Appl. Energy **86** (2009) 2283. http://dx.doi.org/10.1016/j.apenergy.2009.03.022
7. *Shibata, M., Murase, K., Furuya, N.,* J. Appl. Electrochem. **28** (1998) 1121. http://dx.doi.org/10.1023/A:1003451119024
8. *de Vooys, A. C. A., Koper, M. T. M., van Santen, R. A., van Veen, J. A. R.,* J. Catal. **202** (2001) 387. http://dx.doi.org/10.1006/jcat.2001.3275
9. *Garin, F.,* Appl. Catal. A Gen. **222** (2001) 183. http://dx.doi.org/10.1016/S0926–860X(01)00827–4
10. *Kung, H. H., Kung, M. C., Costello, C. K.,* J. Catal. **216** (2003) 425. http://dx.doi.org/10.1016/S0021–9517(02)00111–2
11. *Chen, Q.-S., Feliu, J. M., Berna, A., Climent, V., Sun, S-G.,* Electrochim. Acta **56** (2011) 5993. http://dx.doi.org/10.1016/j.electacta.2011.04.101
12. *Petrov, K. M.,* GDE for oxidation of SO_2 (in Bulgarian), PhD Thesis, Sofia, 1995.

13. *Haneda, M., Morita, T., Nagao, Y., Kintaichi, Y., Hamada, H.,* Phys. Chem. Chem. Phys. **3** (2001) 4696. http://dx.doi.org/10.1039/B106074K
14. *Haneda, M., Kintaichi, Y., Hamada, H.,* Appl. Catal. B Env. **55** (2005) 169. http://dx.doi.org/10.1016/j.apcatb.2004.08.003
15. *Jansson, J., Skoglundh, M., Fridell, E., Thormählen, P.,* Top. Catal. **16** (1–4) (2001) 385. http://dx.doi.org/10.1023/A:1016681620216
16. *Thormahlen, P., Skoglundh, M., Fridell, E., Andersson, B.,* J. Catal. **188** (1999) 300. http://dx.doi.org/10.1006/jcat.1999.2665
17. *Ji, L., Lin, J., Zeng, H. C.,* J. Phys. Chem. B. **104** (2000) 1783. http://dx.doi.org/10.1021/jp993400l
18. *Solsona, B., Davies, T. E., Garcia, T., Vazquez, I., Dejoz, A., Taylor, S. H.,* Appl. Catal. B Env. **84** (2008) 176. http://dx.doi.org/10.1016/j.apcatb.2008.03.021
19. *Zavyalova, U., Scholz, P., Ondruschka, B.,* Appl. Catal. A Gen. **323** (2007) 226. http://dx.doi.org/10.1016/j.apcata.2007.02.021
20. *Ataloglou, T., Vakros, J., Bourikas, K., Fountzoula, C., Kordulis, C., Lycourghiotis, A.,* Appl. Catal. B Env. **57** (2005) 299. http://dx.doi.org/10.1016/j.apcatb.2004.11.010
21. *Ahmadov, T. O., Durmus, Z., Baykal, A., Kavas, H.,* Inorganic Materials **47** (4) (2011) 426.
22. *Nikolova, V., Iliev, P., Petrov, K., Vitanov, T., Zhecheva, E., Stoyanova, R., Valov, I., Stoychev, D.,* J. Power Sources **185** (2008) 727. http://dx.doi.org/10.1016/j.jpowsour.2008.08.031
23. *Ginberg, A. M.,* Galvanotechika (Handbook – in Russian), Metallurgia Publ. H., Moscow, 1987, pp 87.
24. *Rashkova, V.,* Vacuum deposited Me-Co-Te-O thin films as electrocatalysts for a bifunctional oxygen electrodes (in Bulgarian), PhD Thesis, Sofia, 2006, pp 59.
25. *Scofield, J. H.,* J. Electron. Spectrosc. Rel. Fenom. **8** (1976) 129. http://dx.doi.org/10.1016/0368–2048(76)80015–1
26. *Hori, C. E., Permana, H., Simon Ng, K. Y., Brenner, A., More, K., Rahmoeller, K. M., Belton, D.,* Appl. Catal. B Env. **16** (1998) 105. http://dx.doi.org/10.1016/S0926–3373(97)00060-X
27. *Moulder, J. F., Stickle, W. F., Sobol, P. E., Bomben, K. D.,* Handbook of X-ray Photoelectron Spectroscopy, second ed., Perkin-Elmer Corporation, Eden Prairie, MN, 1992.
28. *Dillard, J. G., Schenck, C., Koppelman, M.,* Clays and Clay Minerals **31** (1983) 69. http://dx.doi.org/10.1346/CCMN.1983.0310112
29. *Yang, J., Liu, H., Martens, W. N., Frost, R. L.,* J. Phys. Chem. C **114** (2010) 111. http://dx.doi.org/10.1021/jp908548f
30. *Barr, T. L.,* J. Phys. Chem. **82** (1978) 1801. http://dx.doi.org/10.1021/j100505a006
31. *Poleunis, C., Weng, L. T., Sclavons, M., Bertrand, P., Franquinet, P., Legras, R., Carlier, V.,* J. Adhesion Sci. Technol. **9** (1995) 859. http://dx.doi.org/10.1163/156856195X00743
32. *Nefedov, V. I., Salyn, Y. V., Leonhardt, G., Scheibe, R.,* J. Electron Spectrosc. Relat. Phenom., **10** (1977) 121. http://dx.doi.org/10.1016/0368–2048(77)85010-X
33. *Stypula, B., Stoch, J.,* Corr. Sci. **36** (1994) 2159. http://dx.doi.org/10.1016/0010–938X(94)90014–0
34. *Tsanev, A., Iliev, P., Petrov, K., Stefanov, P., Stoychev, D.,* Bulg. Chem. Comm., **40** (2008) 348.
35. *Nikolskij, B. P.,* Chemist's Handbook (in Russian), 2nd ed., Vol. 3, Chemistry, Moscow, 1964. Pp. 740, 752.
36. *Rieger, Ph. H.,* Electrochemistry, 2nd. ed., Chapman & Hall, Inc, USA, 1994.
37. *Wagner, C., Traube, W.,* Z. Electrochem. **44** (1938) 293.
38. *de Vooys, A. C. A., Koper, M. T. M., van Santen, R. A., van Veen, J. A. R.,* Electrochim. Acta **46** (2001) 923. http://dx.doi.org/10.1016/S0013–4686(00)00678–2
39. *Boix, A. V., Aspromonte, S. G., Miro, E. E.,* Appl. Catal. A Gen. **341** (2008) 26. http://dx.doi.org/10.1016/j.apcata.2007.12.032
40. *Tao, F., Gao, C., Wen, Z., Wang, Q., Li, J., Xu, Z.,* J. Solid State Chem. **182** (2009) 1055. http://dx.doi.org/10.1016/j.jssc.2009.01.030
41. *Pal, J., Chauhan, P.,* Mat. Charact. **61** (2010) 575. http://dx.doi.org/10.1016/j.matchar.2010.02.017
42. *Greenwood, N. N., Earnshaw, A.,* Chemistry of the Elements, 2nd ed., Butterworth-Heinemann, Oxford, 1997, pp. 1117.